The association of cusp-aligned arcs with plasma in the magnetotail implies a closed magnetosphere

S. E. Milan[1]*, M. K. Mooney[1], G. E. Bower[1], M. G. G. T. Taylor[2], L. J. Paxton[3], I. Dandouras[4], A. N. Fazakerley[5], C. M. Carr[6], B. J. Anderson[7], and S. K. Vines[7]

[1]School of Physics and Astronomy, University of Leicester, Leicester, UK.
[2]ESA/ESTEC, Noordwijk, The Netherlands.
[3]William B. Hanson Center for Space Sciences, University of Texas at Dallas, USA.
[4]Institut de Recherche en Astrophysique et Planétologie (IRAP), CNRS and Université Paul Sabatier, Toulouse, France.
[5]Mullard Space Science Laboratory, University College, London, UK.
[6]Imperial College, London, UK.
[7]Johns Hopkins University, Applied Physics Laboratory, USA.

Key Points:

- Cusp-aligned arcs observed by the DMSP spacecraft occur frequently for northward IMF
- Cluster and Geotail observations show that the arcs are accompanied by trapped plasma at high latitudes in the magnetotail
- We interpret cusp-aligned arcs as a signature of a magnetosphere almost entirely closed by dual-lobe reconnection

*School of Physics and Astronomy, University of Leicester, Leicester LE1 7RH, UK

Corresponding author: Steve Milan, `steve.milan@le.ac.uk`

Abstract

We investigate a fifteen-day period in October 2011. Auroral observations by the SSUSI instrument onboard the DMSP F16, F17, and F18 spacecraft indicate that the polar regions were covered by weak cusp-aligned arc emissions whenever the IMF clock angle was small, $|\theta| < 45°$, which amounted to 30% of the time. Simultaneous observations of ions and electrons in the tail by the Cluster C4 and Geotail spacecraft showed that during these intervals dense (≈ 1 cm^{-3}) plasma was observed, even as far from the equatorial plane of the tail as $|Z_{GSE}| \approx 13\ R_E$. The ions had a pitch angle distribution peaking parallel and antiparallel to the magnetic field and the electrons had pitch angles that peaked perpendicular to the field. We interpret the counter-streaming ions and double loss-cone electrons as evidence that the plasma was trapped on closed field lines, and acted as a source for the cusp-aligned arc emission across the polar regions. This suggests that the magnetosphere was almost entirely closed during these periods. We further argue that the closure occured as a consequence of dual-lobe reconnection at the dayside magnetopause. Our finding forces a significant re-evaluation of the magnetic topology of the magnetosphere during periods of northwards IMF.

Plain Language Summary

The magnetosphere is usually assumed to contain both open and closed magnetic flux. Closed magnetic field lines have both ends connected to the Earth; open field lines connect to the Earth at one end and into the interplanetary medium at the other. There tends to be little plasma on open field lines as the particles escape down the magnetotail, whereas plasma on closed field lines is trapped. Open flux near the poles naturally explains the oval configuration of Earth's auroras, with a lack of auroras at very high latitudes where there is no plasma to cause emissions. Somewhat unexpectedly, we show that auroral emission near the poles is common and that at these times there is significant plasma in the magnetotail, indicating that the magnetosphere contains only closed flux. We propose that this magnetic configuration is formed by a process known as dual-lobe magnetic reconnection which occurs when the interplanetary magnetic field within the solar wind points northwards. We must re-evaluate the standard picture of magnetospheric structure during these periods of northwards interplanetary magnetic field.

1 Introduction

In this study we investigate repeated occurrences of cusp-aligned arcs (CAAs), the poorly understood situation in which weak auroral emissions fill the polar regions, during a fifteen-day interval in 2011. We conclude that CAAs are a common occurrence during periods of northward interplanetary magnetic field (IMF), and that they are a signature of a nearly- or entirely-closed magnetosphere. This forces a significant re-evaluation of the magnetic topology of the magnetosphere during northward IMF.

The coupling between the solar wind and the magnetosphere is relatively well understood for southward-directed IMF: as first proposed by Dungey (1961), magnetic reconnection near the subsolar magnetopause opens previously-closed magnetic flux which then forms the magnetotail lobes; thereafter, magnetic reconnection in the central plane of the tail recloses flux which returns to the dayside, resulting in the Dungey cycle of magnetospheric convection. The northern and southern ionospheric polar caps, the dim regions encircled by the auroral ovals, are the ionospheric projection of the open flux forming the lobes, and their size can be used to quantify the open flux content of the magnetosphere, F_{PC} (e.g., Milan et al., 2003). This naturally explains many aspects of magnetospheric structure and dynamics, including the formation of the magnetotail, the twin-cell ionospheric convection pattern, the morphology of the auroral oval, the plasma populations within the magnetosphere, and the evacuated magnetotail lobes. When time-varying magnetic reconnection rates are considered, the expanding/contracting nature

of the polar cap and the substorm cycle can be understood (Siscoe & Huang, 1985; Cowley & Lockwood, 1992; Lockwood & Cowley, 1992). Typically, F_{PC} varies between 0.3 and 0.9 GWb (Milan et al., 2003, 2007, 2021). However, it can become as low as 0.2 GWb ($\sim 2.5\%$ of the 8 GWb associated with the terrestrial dipole) during particularly extreme nightside reconnection events, accompanied by a near-total in-filling of the polar regions by bright auroral emission (e.g., Milan et al., 2004). In this paper we show that in fact the polar cap closes entirely, frequently, and with much less fanfare, during periods of northwards IMF.

The coupling during northward-directed IMF is still poorly understood. Although Dungey (1963) correctly proposed that magnetic reconnection would take place at the high latitude magnetopause, tailwards of the cusps, the ramifications are still not fully resolved. The list of northward-IMF (IMF $B_Z > 0$ or NBZ) phenomena includes: single- and dual-lobe reconnection (e.g., Cowley, 1981; Fuselier et al., 2012), reverse convection in the polar cap (e.g., Huang et al., 2000), NBZ field-aligned currents poleward of the noon auroral oval (e.g. Iijima et al., 1984), cusp auroral spots (e.g., Milan et al., 2000; Frey et al., 2002; Frey, 2007; Carter et al., 2018, 2020), transpolar or polar cap arcs (e.g., Frank et al., 1982; Cumnock et al., 2002; Kullen et al., 2002; Milan et al., 2005; Fear et al., 2014), horse-collar auroras (e.g., Hones Jr et al., 1989; Milan, Carter, Bower, et al., 2020; Bower, Milan, Paxton, & Anderson, 2022), and cusp-aligned arcs (e.g., Y. Zhang et al., 2016; Q.-H. Zhang et al., 2020; Milan et al., 2022; Wang et al., 2023). The interested reader is directed to the recent reviews of NBZ phenomena by Hosokawa et al. (2020) and Fear (2021).

A key question regarding periods of NBZ is the degree to which the magnetosphere loses open magnetic flux, and the resulting distribution of open and closed flux in the polar regions. It has been suggested that polar cap arcs may be associated with both open and closed magnetic flux (e.g., Carlson & Cowley, 2005; Reidy et al., 2020; Bower, Milan, Paxton, & Imber, 2022). Evidence suggests that the most prominent of polar cap arcs, those also known as theta auroras, are likely associated with closed magnetic flux (Fear et al., 2014; Fryer et al., 2021; Coxon et al., 2021), proposed to be produced by magnetic reconnection in the magnetotail (Milan et al., 2005; Fear & Milan, 2012a, 2012b). The situation regarding less prominent sun-aligned or cusp-aligned arcs, in which multiple weak arcs fill the polar regions (Y. Zhang et al., 2016), is as yet unresolved. If these form on the open flux of the largely-evacuated magnetotail lobes, then the source of the auroral precipitation is called into question, though Carlson and Cowley (2005) proposed that polar rain could provide sufficient plasma to be accelerated in flow shears in the ionospheric convection pattern to produce such arcs.

During prolonged NBZ, the polar cap can contract and become teardrop-shaped, leading to the horse-collar auroras (HCAs) configuration (Hones Jr et al., 1989). Milan, Carter, Bower, et al. (2020) and Bower, Milan, Paxton, and Anderson (2022) have suggested that this is formed by the closure of magnetic flux by dual-lobe reconnection (DLR) for near-zero IMF clock angle, supported by numerical simulations (Wang et al., 2023). Dual-lobe reconnection should be an efficient mechanism by which the magnetosphere can capture solar wind plasma (e.g., Imber et al., 2006), and it has been proposed that over time this can lead to the formation of a cold, dense plasma sheet (CDPS) (Øieroset et al., 2005). However, this is not the only means by which solar wind plasma is thought to enter the magnetosphere during periods of NBZ, with inward diffusion at the magnetotail flanks (see discussion in Taylor et al., 2008) or direct entry through (single) lobe reconnection (Shi et al., 2013; Mailyan et al., 2015) being other commonly discussed mechanisms. It is unclear, however, how efficient diffusion can be, how quickly captured solar wind plasma can be redistributed throughout the magnetosphere, and why the plasma remains near the Earth and does not escape back to the solar wind down the open field lines of the lobes, as it does for southwards IMF.
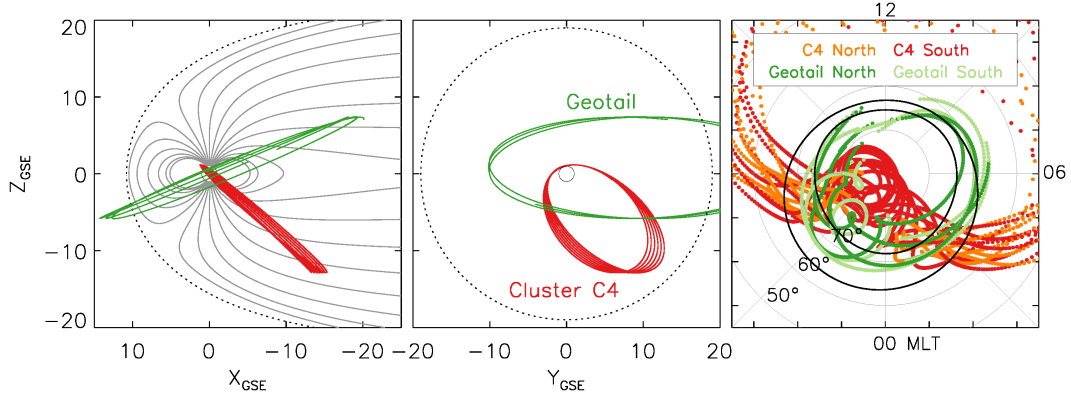
Figure 1. (Left) The orbit of Cluster C4 (red) and Geotail (green) for the period of study, in the GSE $X - Z$ plane. The T96 magnetic field configuration on DOY 280, 2011, at 13 UT, for $P_{dyn} = 2$ nPa, $D_{st} = -10$ nT, $B_Y = 0$ and $B_Z = 5$ nT is superimposed in grey. (Middle) The orbit of Cluster and Geotail for the period of study, in the GSE $Y - Z$ plane; the location of the magnetopause at $X = -10$ R_E is shown for reference. (Right) Field-line tracing from the location of Cluster and Geotail to the northern (orange and dark green) and southern (red and light green) hemisphere ionospheres for the period of interest, presented on a geomagnetic latitude and MLT grid. An average auroral oval for $K_P = 1$ is overlaid for reference.

The cusp-aligned arcs (hereafter CAAs) auroral configuration is perhaps the most poorly-studied NBZ auroral phenomenon. Partially, this is because the emissions tend to be weak, so are better observed from the ground (e.g., Ismail et al., 1977; Hosokawa et al., 2011), with limited geographical coverage, rather than from space. Recently, Q.-H. Zhang et al. (2020) and Wang et al. (2023) suggested that CAAs are produced by plasma flow shears introduced into the magnetosphere by Kelvin-Helmholtz surface waves excited on the magnetotail flanks by the flow of the solar wind. However, this does not resolve the source of the precipitating plasma. On the other hand, Milan et al. (2022) proposed that if DLR continues for a prolonged period, then the magnetosphere can become almost entirely closed and the horse-collar auroral configuration can develop to the point where the polar slot (distorted polar cap) can almost disappear. In this scenario, the closed magnetosphere will be filled with trapped solar wind plasma and, according to Milan et al. (2022), flow shears produced by lobe reconnection can then accelerate this trapped plasma into the atmosphere to form the CAAs. Whereas Carlson and Cowley (2005) suggested that the source of plasma to produce weak polar cap arcs was polar rain that had fled to the distant magnetotail along open field lines, instead Milan et al. (2022) proposed that the source is solar wind plasma captured by DLR and trapped closer to the Earth on closed field lines.

In this study we examine plasma populations observed in the near-Earth tail by the C4 spacecraft of the Cluster constellation (Escoubet et al., 2001) and the Geotail (Nishida, 1994) spacecraft during a prolonged period in October 2011 when auroral observations from F16, F17, and F18 of the Defense Meteorological Spacecraft Program detected multiple instances of CAAs. Dense plasma is repeatedly found in regions that would normally be occupied by the evacuated open field lines of the northern and southern lobes, and it is concluded that the magnetosphere is almost entirely closed and the plasma is trapped, providing a source for the high latitude auroral emission.

2 Observations

The period under investigation is the 3 to 17 October 2011 (days-of-year 276 to 290), which encompasses six orbits of the Cluster constellation during its tail season and three orbits of Geotail; the orbits are shown in Figure 1. At this time, the orbit of C4 was inclined such that it was southwards of the neutral sheet for most of the time, except near perigee. During the study interval, C4 reached $Z_{GSE} \approx -13\ R_E$, $X_{GSE} \approx -14\ R_E$ at apogee, and it was located relatively centrally in the tail, $0 < Y_{GSE} < 10\ R_E$, in the first half of each orbit, but closer to the dusk flank in the second. The orbit of Geotail was such that it sampled the magnetotail northwards of the neutral sheet, up to $Z_{GSE} \approx 8\ R_E$ at $X_{GSE} \approx -19\ R_E$. A representative magnetic field tracing in the T96 model (Tsyganenko, 1995), with input parameters $P_{dyn} = 2$ nT, $D_{st} = -10$ nT, and IMF $B_Y = 0$ and $B_Z = 5$ nT, is overlaid for reference. These parameters were chosen to represent a quiet NBZ magnetosphere, and will be used throughout the rest of the study to compare with magnetic field observations. As the plasma sheet is usually confined to $|Z| < 5\ R_E$, for much of their orbits Geotail and C4 are expected to be within the northern and southern lobes of the magnetotail, respectively. Field line tracings from the locations of the two spacecraft to the northern and southern ionospheres are also presented, with a $K_P = 1$ average auroral oval superimposed for reference. This indicates that near apogee C4 would normally be expected to map to the central polar cap in the southern hemisphere, and that Geotail would frequently map to the nightside polar cap in the northern hemisphere.

Auroral observations during this period are provided by the Special Sensor Ultraviolet Spectrographic Imager or SSUSI experiment (Paxton et al., 1992) onboard the DMSP-F16, -F17, and -F18. The DMSP spacecraft have sun-synchronous orbits near an altitude of 850 km. SSUSI measured auroral luminosity in a swath either side of the spacecraft orbit in the Lyman-Birge-Hopfield short (LBHs) band, 140 to 150 nm (see Paxton and Zhang (2016); Paxton et al. (2017, 2021) and the references cited therein for further description of the instrument and data products). Measurements of the distribution of magnetosphere-ionosphere field aligned currents (FACs) were provided by the Active Magnetosphere and Planetary Electrodynamics Response Experiment (AMPERE) technique (Anderson et al., 2000; Coxon et al., 2018; Waters et al., 2001). We also make use of ionospheric flow observations provided by the Super Dual Auroral Radar Network (SuperDARN (Chisham et al., 2007)) and the Ion Driftmeter (IDM) component of the Special Sensors–Ions, Electrons, and Scintillation thermal plasma analysis package or SSIES instrument onboard the Defense Meteorological Satellite Program spacecraft (DMSP/IDM (Rich & Hairston, 1994)). Solar wind parameters were taken from the OMNI data-set (King & Papitashvili, 2005).

Figure 2 shows 12 snapshots of the auroral morphology from DOYs 278 to 280. Below this, a keogram of the observations along the dawn-dusk meridian made by DMSP-F16/SSUSI in the northern hemisphere is shown, along with the IMF clock angle from OMNI. Around 10:20 UT on DOY 278 (panels a and b), the IMF had a southwards component and typical twin-cell ionospheric flows were observed by SuperDARN and DMSP/IDM (not shown for brevity). The auroral morphology was also typical, showing an oval surrounding a dim polar cap, with evidence for substorm activity on the nightside. Between approximately 16:00 UT, DOY 278, and 13:00 UT, DOY 279, the IMF turned northwards. During this period the auroras dimmed, contracted to higher latitudes and acquired a horse-collar auroral configuration, before the polar regions filled with auroral emission mainly in the form of cusp-aligned arcs or CAAs (c to f). CAAs are seen in both northern and southern hemispheres, panels c and e being from the north and d and f being from the south. Then the IMF turned southwards again, twin-cell convection resumed, and the polar cap reopened (g and h). There followed another period of NBZ, during which CAAs reformed (i and j), before again a southward turning and a reopening of the polar cap (k to l). The lower panels clearly show the expansions and contractions
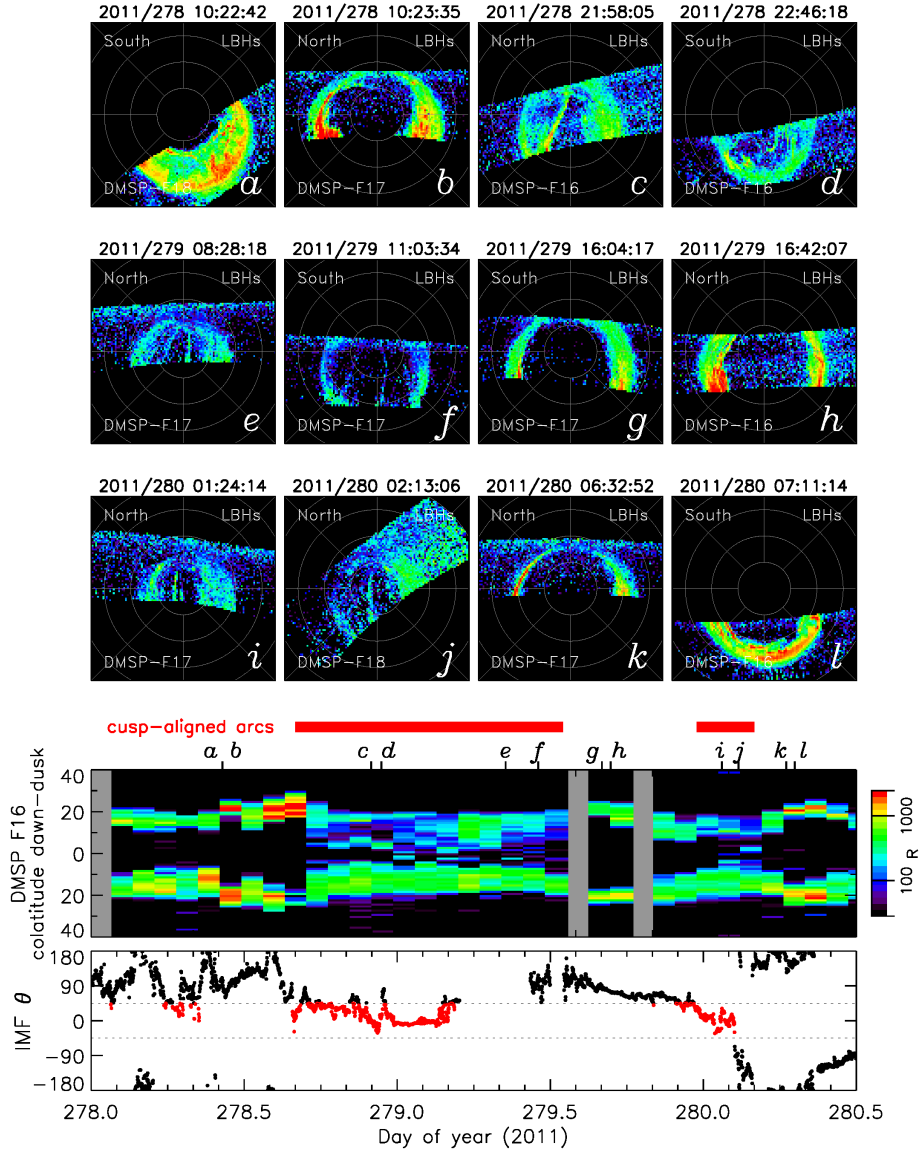
Figure 2. Snapshots of the LBHs auroral configuration in the northern and southern hemispheres observed by DMSP/SSUSI onboard DMSP-F16, -F17, and -F18 between 5 and 7 October 2011. Each panel is presented in a geomagnetic latitude and local time format, with noon towards the top and dawn towards the right. Grey circles indicate geomagnetic latitude in steps of 10°. Of the two lower panels, the top one shows a keogram of auroral emissions observed by DMSP-F16/SSUSI along the dawn-dusk meridian of the northern hemisphere; grey vertical bars indicate where data is missing. Red horizontal bars indicate the times that cusp-aligned arcs were observed. The bottom panel is clock angle, highlighted in red when $|\theta| < 45°$.

of the auroral oval with changes in clock angle, and the presence of auroral emissions at high latitudes during periods when the clock angle is near zero, $|\theta| < 45°$, highlighted in red.

Over the rest of the period considered several other intervals of CAAs were found, as will be indicated in later figures. The start and end times of these intervals are approximate due to the relatively coarse cadence of the DMSP orbits; there are also periods when it was not possible to positively identify whether CAAs were present or not, due to only partial coverage of the polar regions by the SSUSI field-of-view. During periods when HCAs or CAAs were present, the ionospheric flows measured by SuperDARN and DMSP/IDM and the field-aligned currents observed by AMPERE were consistent with the observations reported by Milan, Carter, Bower, et al. (2020) and Milan et al. (2022) – reverse lobe convection, NBZ FACs at noon – suggesting that dual-lobe reconnection was responsible for closing the magnetosphere. The occurrence of CAAs when $|\theta| < 45°$ is also consistent with the statistical occurrence of horse-collar auroras (Bower, Milan, Paxton, & Anderson, 2022), thought to be the auroral precursor to CAAs.

We use Cluster C4 observations from the Composition and Distribution Function analyser of the Cluster Ion Spectrometry instrument (C4/CIS-CODIF (Rème et al., 1997)), the Plasma Electron And Current Experiment (C4/PEACE (Johnstone et al., 1997)), and the Fluxgate Magnetometer (C4/FGM (Balogh et al., 1997)). Figure 3 covers the period 3 to 9 October, spanning the first three C4 orbits considered and encompassing the interval shown in Figure 2. The panels are presented in the following order. (a) The GSE X, Y, and Z (R_E) position of C4. (b) The B_X, B_Y, B_Z components of the magnetic field measured by C4/FGM in GSE coordinates. Dots indicate predications of the magnetic field measurements by the T96 (Tsyganenko, 1995) model, with fixed inputs (as before). (c) The proton density, n_i, observed by C4/CIS-CODIF. Vertical red bars indicate when CAAs were observed by DMSP/SSUSI. (d) The proton differential energy flux spectrogram measured by C4/CIS-CODIF. (e) The electron differential energy flux spectrogram measured by C4/PEACE. (f) A dawn-dusk keogram of auroral emissions observed by DMSP-F16/SSUSI in the northern hemisphere. (g) A dawn-dusk keogram of FAC density measured by AMPERE in the northern hemisphere, with red/blue indicating up/down currents. (h) The clock angle of the IMF, θ, highlighted in red when $|\theta| < 45°$. (i) The GSM B_X, B_Y, B_Z components of the IMF from OMNI. (j) The solar wind speed and density from OMNI.

The SSUSI keogram (f) reveals that at most times there is little auroral emission inside the auroral oval, consistent with an open polar cap, except at the times of CAAs (red bars in (c)) when $|\theta| < 45°$. The region 1/2 FACs (Iijima & Potemra, 1976) observed by AMPERE (g) are enhanced when the polar cap is open, indicating Dungey cycle driving of the magnetosphere by subolar reconnection, especially during periods with IMF $B_Z < 0$ nT, $|\theta| > 90°$. When CAAs are present the R1/R2 FACs are weak, though NBZ FACs tend to be observed at noon (not shown).

Near the perigee of each orbit (marked PG) when $|Z| < 5\ R_E$, C4 passed through the plasma sheet and ring current regions and enhanced proton densities, n_i, were observed (c). During the first orbit of Figure 3 almost no plasma was observed when $Z < -5\ R_E$, consistent with the open lobe. In contrast, while C4 was near perigee on DOY 278 the IMF turned northwards and CAAs were observed, and throughout this period C4 was engulfed in protons with $n_i \approx 1$ cm^{-3} up to near apogee (AG) on DOY 279. As the IMF turned southwards around 13:00 UT on DOY 279, the density returned to typical lobe values, $n_i < 0.1$ cm^{-3}. Around 00 UT on DOY 280 CAAs were once again observed, and n_i rose to near 1 cm^{-3}, only to drop again at 04 UT as the IMF turned southwards; the IMF remained predominantly southwards for the duration of the third orbit, and n_i remained low throughout (except for a short period near apogee, see below).
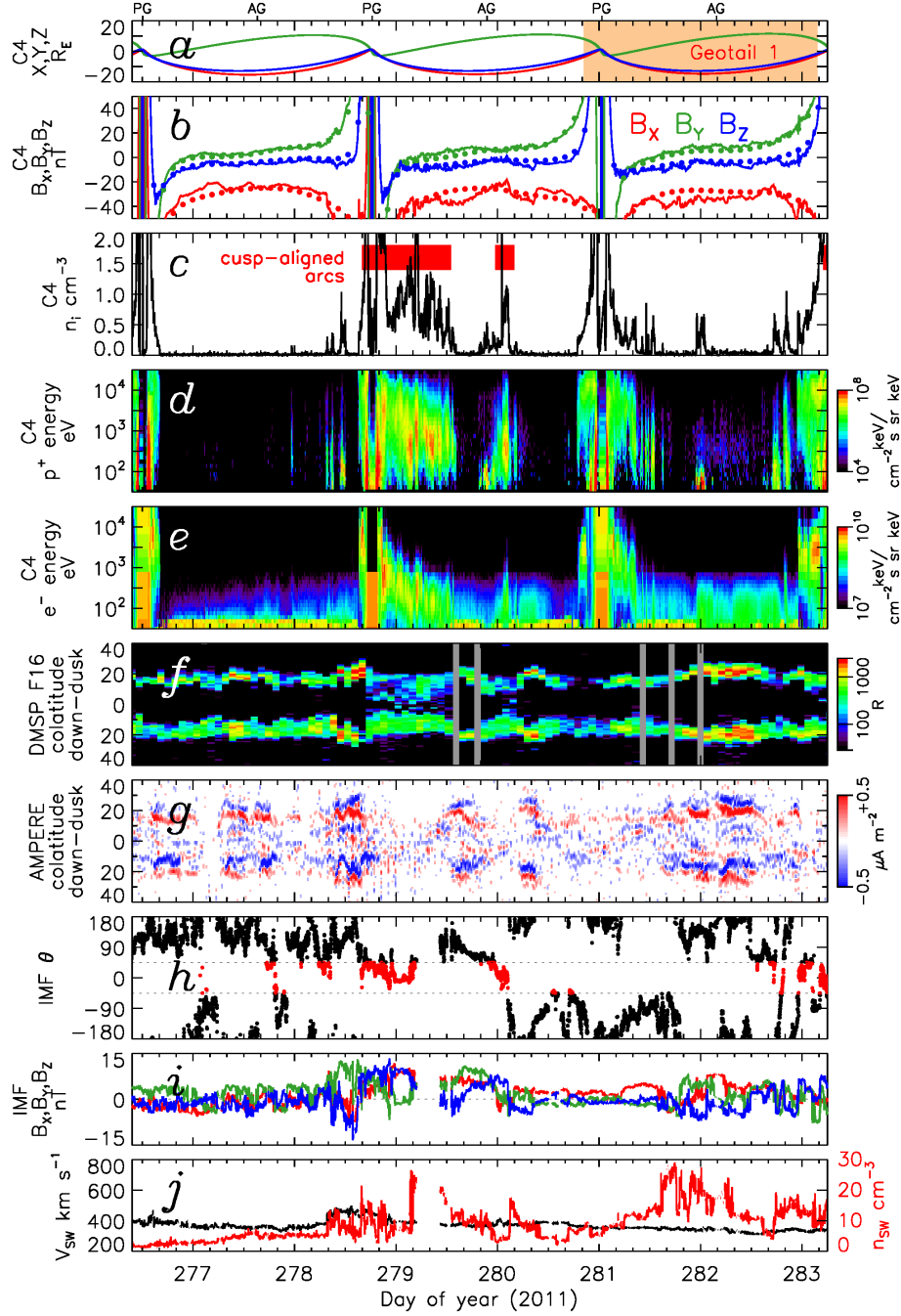
Figure 3. Observations from 3 to 10 October 2011, which encompasses three orbits by Cluster. (*a*) The GSE position of C4. Apogees and perigees of the orbit are indicated by AG and PG. Orange highlighting indicates the time of the first Geotail orbit shown in Figure 6. (*b*) C4/FGM observations of the magnetic field. T96 model predictions for fixed input parameters are indicated as dots. (*c*) C4/CIS-CODIF ion density measurements. Red bars indicate periods of observation of cusp-aligned arcs by DMSP/SSUSI. (*d*) C4/CIS-CODIF ion spectrogram. (*e*) C4/PEACE electron spectrogram. (*f*) A dawn-dusk keogram of auroral observations by DMSP-F16/SSUSI in the northern hemisphere. (*g*) A dawn-dusk keogram of field-aligned currents measured by AMPERE, red and blue being upward and downward FACs, respectively. (*h*) The clock angle of the IMF from OMNI. The clock angle is highlighted in red when $|\theta| < 45°$. (*i*) The components of the IMF from OMNI. (*j*) The solar wind speed and density from OMNI.

The C4/CIS-CODIF spectrogram (d) indicates that the CAA-related ions had energies between several 100s and several 1000s eV. (We note that at the apogees of the second and third orbits a brief interval of cold, < 100 eV, ions was also observed.) The C4/PEACE spectrogram (e) indicates that the ions were accompanied by electrons, with energies below about 1 keV. In the first CAA interval of DOY 279 the ions, and especially the electrons, reduced in energy with time, indicating a cooling of the plasma.

Figure 4 presents the next three orbits of C4. During this period, the IMF $|\theta| < 45°$ for much of the time, and there were several intervals of CAAs observed by DMSP/SSUSI. Accompanying these intervals, C4/CIS-CODIF saw elevated n_i, where otherwise lobe conditions might have been expected. During DOYs 287 to 290, there were repeated swings between $|\theta| < 45°$ and $|\theta| > 45°$, and CAAs and protons came and went in tandem.

Figure 5 focusses on the two intervals of CAAs presented in Figures 2 and 3. In addition to the spectrograms, pitch angle distributions of the ions (d) and electrons (f) are shown. The proton pitch angle fluxes are integrated across the full energy range of the CIS-CODIF instrument; the electron fluxes are calculated from the low energy electron analyser head of the PEACE instrument, limited to energies above 100 eV to remove the contribution of photoelectrons. During periods of CAAs, and when C4 was not too close to the Earth, ion pitch angles were concentrated at $0°$ and $180°$, indicating two counter-streaming populations. The electron pitch angles, conversely, peaked at $90°$, with a distinct lack of electrons near $0°$ and $180°$, indicating a double loss-cone distribution. The double loss-cone electron distribution is similar to that observed by Fear et al. (2014) above a transpolar arc, and is indicative of plasma trapped on closed field lines. The counter-streaming ions support this conclusion. We note that the ion and electron densities during the periods of CAAs were quite variable, indicating that the trapped plasma was not uniformly distributed but was present continuously. The solar wind density was variable during this period, but it is not clear if variations in ion/electron density and energy observed by C4 are correlated with enhancements in n_{SW}. As noted previously, the ion and electron energies decreased overall with time, which might indicate the progressive mixing of plasma sheet and solar wind populations, leading to the formation of a cold, dense plasma sheet (e.g., Øieroset et al., 2005).

Just prior to the second period of CAAs, CIS-CODIF detected a beam of low energy ions observed only near $0°$ pitch angles (i.e. flowing tailward). A similar beam was observed around 00 UT near apogee on DOY 282 (see Figure 3). As there are no counter-streaming ions, we suggest that at these are the signature of plasma escaping to the solar wind along open field lines.

Superimposed on the C4/FGM observations (a) is a model prediction from T96 for fixed NBZ input parameters (as before). The model tends to match the observations well during the periods of CAAs, but the B_X component was enhanced by ≈ 10 nT during the periods when CAAs were not present, indicating that the tail was more inflated at these times. This also supports the conclusion that the magnetotail open flux was significantly reduced when CAAs were observed.

Figure 6 presents two time intervals when Geotail was located in the magnetotail; Figures 3 and 4 show that these roughly correspond to orbits 3 and 5 of C4. Panels a and b show that in each case Geotail entered the dusk flank of the magnetotail at the start of the interval, near $Z \approx 5 R_E$, and rose to $Z \approx 8 R_E$ at $X \approx -19 R_E$, $Y \approx 0 R_E$. It later exited the dayside magnetopause in the pre-noon sector. Panels e to l present ion and electron spectrograms from the Low Energy Particle (LEP) instrument (Mukai et al., 1994), showing fluxes in the sunward and tailward directions. During the first orbit, the plasma sheet was seen as the spacecraft entered and exited the magnetosphere, but the evacuated lobe was encountered from 16 UT on DOY 281 to 14 UT on DOY 282. During this period, IMF $|\theta| > 45°$ at all times (m). During the second orbit, the plasma sheet was also seen at the start and the end, with periods of lobe between 23 UT, DOY
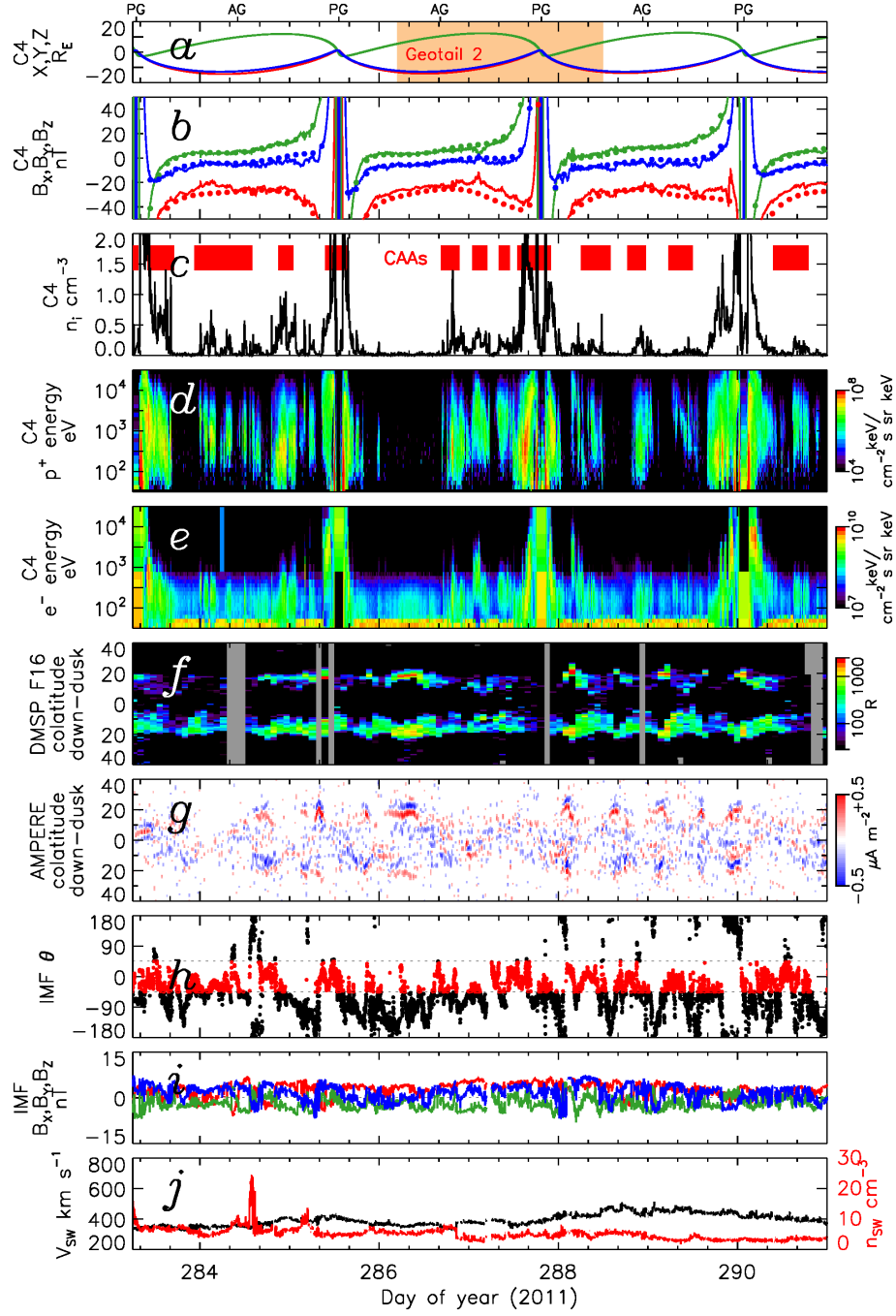
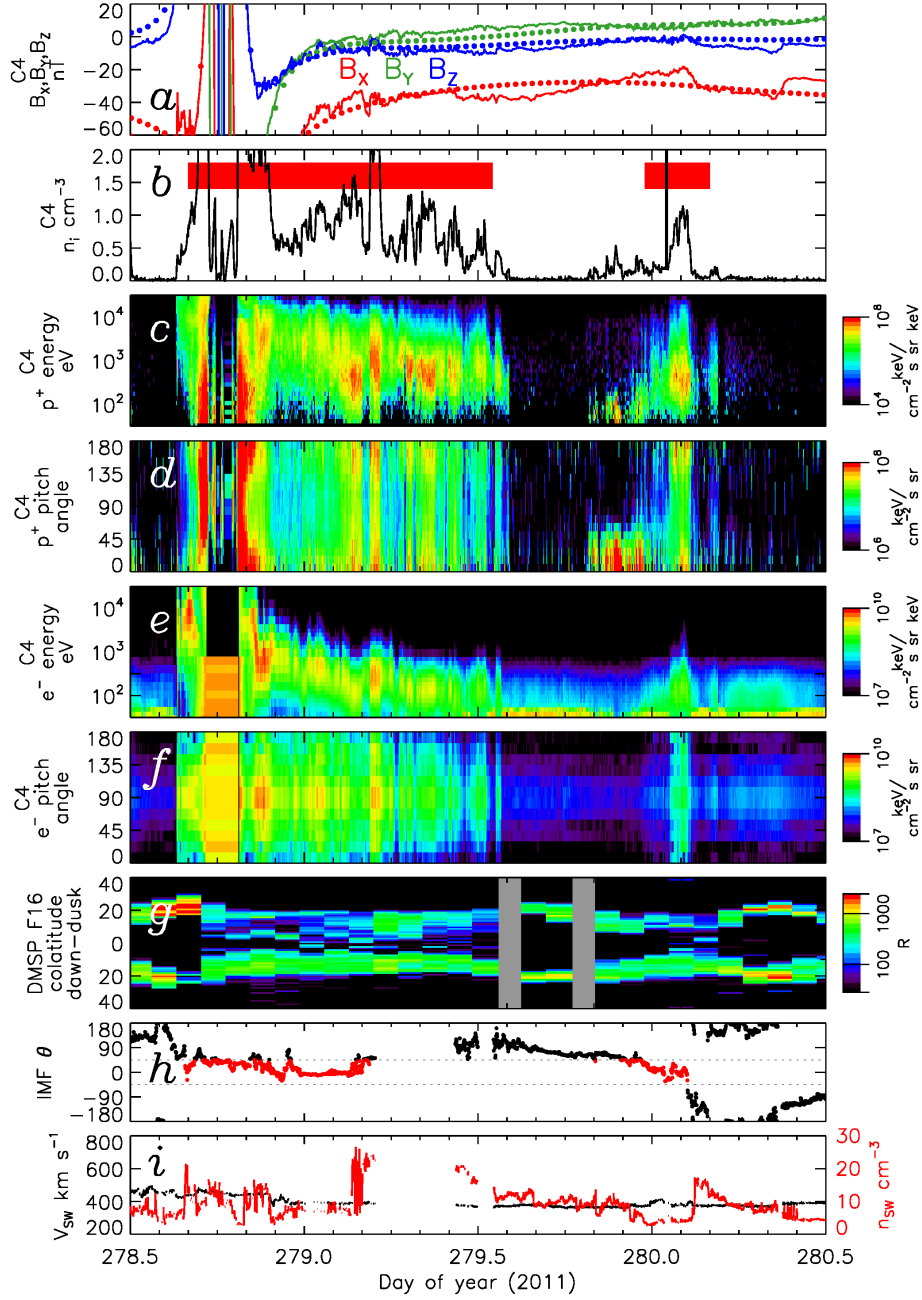**Figure 4.** Observations from 10 to 17 October, presented in the same format as Figure 3.

Figure 5. Observations from 5 to 7 October 2011. (*a*) C4/FGM observations of the magnetic field. T96 model predictions for fixed input parameters are indicated as dots. (*b*) C4/CIS-CODIF ion density measurements. Red bars indicate periods of observation of cusp-aligned arcs by DMSP/SSUSI. (*c*, *d*) C4/CIS-CODIF ion spectrogram and pitch angle distribution. (*e*, *f*) C4/PEACE spectrogram and pitch angle distribution. (*g*) A dawn-dusk keogram of auroral observations by DMSP-F16/SSUSI. (*h*) The clock angle of the IMF from OMNI. The clock angle is highlighted in red when $|\theta| < 45°$. (*i*) The solar wind speed and density from OMNI.
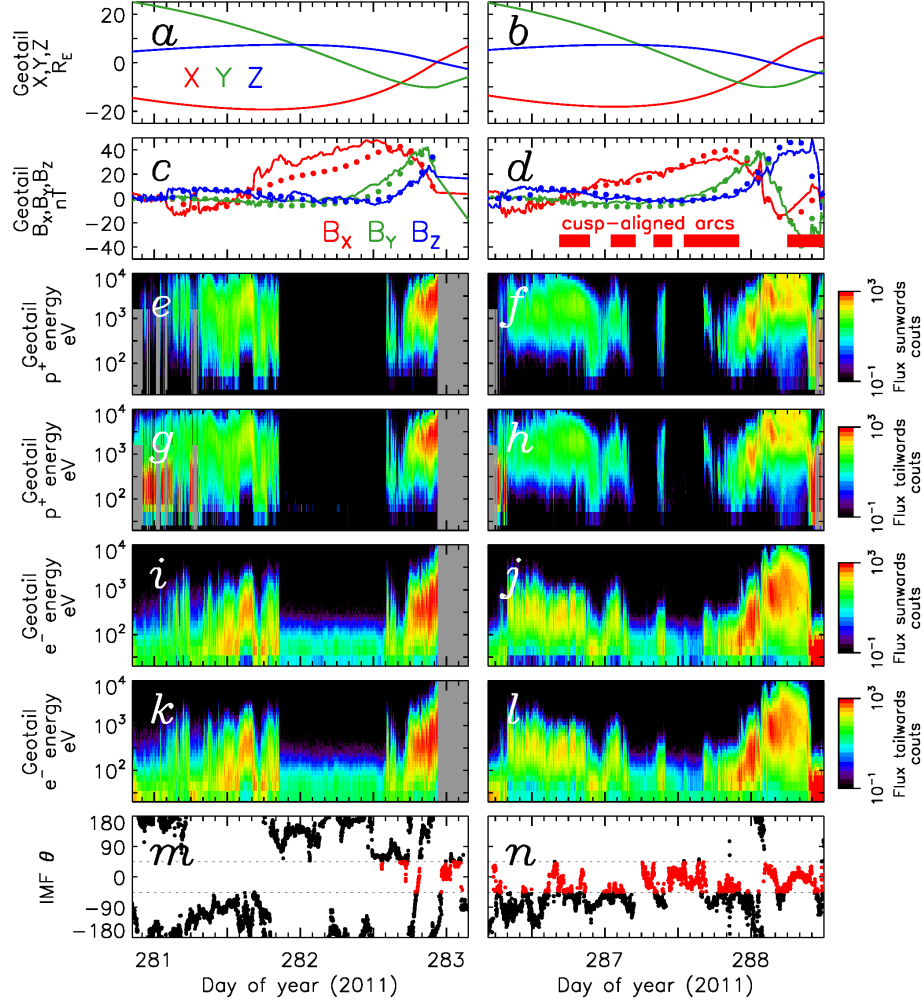
Figure 6. Two time periods during which Geotail was located within the magnetotail. (*a*, *b*) The GSE location of Geotail. (*c*, *d*) The magnetic field components measured by MGF, with a T96 prediction superimposed. Red bars indicate when cusp-aligned arcs were observed by DMSP/SSUSI. (*e*, *f*) Ion spectrograms of fluxes in the sunwards direction. (*g*, *h*) Ion spectrograms of fluxes in the tailwards direction. (*i*, *j*) Electron spectrograms of fluxes in the sunwards direction. (*k*, *l*) Electron spectrograms of fluxes in the tailwards direction. (*m*, *n*) IMF clock angle, highlighted in red when $|\theta| < 45°$.

286, and 18 UT, DOY 287. However, three intervals of plasma, with fluxes in both the sunwards and tailwards directions, were detected at the same time as CAAs were observed by DMSP/SSUSI, associated with excursions to $|\theta| < 45°$ (n). Plasma was also seen by C4 in the southern tail at these times (Figure 4), and the plasma characteristics were similar. The presence of fluxes in both the sunwards and tailwards directions, indicate that the plasma is trapped on closed field lines. During the second orbit, the magnetic field observed by the Magnetic Field Experiment (MGF) instrument (Kokubun et al., 1994), panel d, matched closely the prediction by T96. However, during the first orbit, around the time Geotail was in the lobe the B_X component was elevated above the prediction (c) indicating an inflated magnetotail.

3 Discussion

The occurrence of cusp-aligned arcs filling the polar regions is frequent. We find that CAAs have a high probability of appearing if $|\theta| < 45°$ for an appreciable length of time (one to two hours or more). During our period of study, CAAs were observed for approximately 30% of the time. Although polar cap arcs received attention in the past (e.g., Ismail et al., 1977), CAAs are too dim to have been detected by previous generations of global auroral imagers (e.g., IMAGE FUV), so their importance has been overlooked. We find that CAAs are accompanied by dense plasma of energies from several eV to several 10s keV in regions of the magnetosphere (up to $|Z| \approx 13$ R_E in our observations) that would normally be occupied by the evacuated tail lobes. Shi et al. (2013) interpreted similar observations of such plasma in the "lobes" as an indication of direct ingress of solar wind plasma via (single) lobe reconnection. However, it seems unlikely that this plasma should reside in the near-Earth tail for long, rather than disappearing down the tail along open field lines, as occurs during periods of southwards IMF. Instead, we suggest that this plasma must be trapped on closed field lines. This interpretation is supported by the presence of a double loss-cone in the C4 electron pitch angle distributions, similar to the plasma characteristics seen by Fear et al. (2014) at high Z over a transpolar arc. In that case, the plasma was only observed by Cluster on field lines that mapped to the arc, and evacuated lobe was seen to either side; in our case the plasma is observed for prolonged periods (sometimes many hours) wherever C4 is located in the tail. The double loss-cone indicates that the plasma has interacted significantly with the atmosphere in both the northern and southern hemispheres over multiple bounces. The presence of counter-streaming ions observed by C4 is also consistent with closed field lines and trapped plasma, as are the sunwards/tailwards fluxes observed by Geotail: if the magnetic field was open, only tailward fluxes would be expected. This trapped plasma is observed in both the northern and southern portions of the magnetotail, at $Z \approx 8$ R_E and $Z \approx -13$ R_E, simultaneously (see Figures 4 and 6).

Several mechanisms have been proposed by which plasma enters the tail during NBZ conditions, and whether or not it is trapped (e.g., Taylor et al., 2008; Shi et al., 2013). Milan, Carter, Bower, et al. (2020) argued that dual-lobe reconnection explains both the capture and trapping of plasma, and the ionospheric flow pattern and auroral evolution observed during the formation of horse-collar auroras (HCAs), and by extension CAAs (Milan et al., 2022). It also explains the necessity for near-zero clock angle, $|\theta| < 45°$, for the appearance of HCAs (Bower, Milan, Paxton, & Anderson, 2022) and CAAs (this study). We suggest now that this also explains why the polar cap closes and the tail loses its northern and southern lobes, explaining trapped plasma on field lines that map to what would normally be the central polar cap.

We note that between 22 UT, DOY 285, and 08 UT, DOY 286, there were two brief swings of the clock angle to $|\theta| < 45°$, but no CAAs were detected and open lobe was observed by C4 (see Figure 4). This suggests that there is a minimum duration of DLR of one to two hours for plasma to be trapped. This minimum will be related to the reconnection rate, that is the rate at which flux is closed, such that open lobe is replaced

by closed flux containing trapped solar wind plasma. Detailed measurement of the rate of closure, difficult with low cadence DMSP/SSUSI images, will be required to further understand this. However, ionospheric convection measurements (e.g., Chisham et al., 2004, 2008) should help quantify the reconnection rate.

The plasma trapped by DLR then acts as a source for precipitation to produce auroral emission in the polar regions. As shown by Q.-H. Zhang et al. (2020) and Milan et al. (2022), CAAs are produced by inverted-V precipitation, electrons accelerated to energies of a few keV, at shears in the ionospheric convection flow which are associated with upwards field-aligned currents due to converging ionospheric electric fields. This is consistent with the trapped electron population found in this study: in the magnetotail the electrons have energies primarily below one keV and the electron pitch angle distribution has empty loss cones. These electrons will not precipitate without the acceleration provided by flow shears. Once accelerated, the electrons are seen to have energies of several keV in the ionosphere. Precipitating ions with energies of one to several keV are also observed in the ionosphere when CAAs are present, especially towards the nightside, consistent with the trapped ions found in this study. Whereas Carlson and Cowley (2005) proposed that weak polar cap arcs, perhaps indeed CAAs, are produced by accelerated polar rain on open field lines, in our scenario trapped solar wind plasma on closed field lines is the more readily available source population.

On the large scale the ionospheric flow pattern has reverse lobe convection cells, consistent with dual-lobe reconnection (Milan et al., 2022), though on smaller scales multiple flow shears are seen, associated with the CAAs. Q.-H. Zhang et al. (2020) and Wang et al. (2023) suggested that these flow shears are produced by Kelvin-Helmholtz waves on the magnetospheric flanks propagating into the magnetotail. However, the cusp-aligned nature of the arcs shows that the flow shears are also cusp-aligned, which is not necessarily predicted by the KHI mechanism. Instead, Milan et al. (2022) proposed that the flow shears are excited by temporally- and spatially-varying lobe reconnection rates, which explains why the flows and shears naturally radiate from the cusp region. We prefer this latter explanation: lobe reconnection explains the closure of magnetic flux and the trapping of solar wind plasma, it explains the "reverse" flow pattern observed in the ionosphere, it explains the structuring of the auroral precipitation into multiple arcs, and it also explains why the arcs are "cusp-aligned". That the field is closed at high latitudes also explains why CAAs are generally seen in both hemispheres simultaneously (see Figure 2 and Milan et al. (2022)), whereas other polar cap auroral phenomena are not always conjugate (e.g., Reidy et al., 2020; Bower, Milan, Paxton, & Imber, 2022).

That auroral emission is observed across the polar regions suggests that the magnetosphere is almost entirely closed, though it might be expected that open and closed flux is interspersed (Milan et al., 2022). As proposed by Milan et al. (2022), horse-collar auroras are the preliminary stage in the development of CAAs, forming when dual-lobe reconnection first commences (Milan, Carter, Bower, et al., 2020). In other words, it is possible that HCAs form frequently (Bower, Milan, Paxton, & Anderson, 2022) but do not necessarily fully evolve into CAAs if the IMF turns away from near-zero clock angles. The high-latitude arcs which sit at the dawn and dusk edges of the polar slot of the HCA configuration are dimmer than the main auroral oval (Bower, Milan, Paxton, & Anderson, 2022), but are still bright enough to be seen with global auroral imagers (Cumnock & Blomberg, 2004) and can be misinterpreted as transpolar arcs (Milan, Carter, Bower, et al., 2020). However, these HCA arcs are in general brighter than CAAs and so may be detected more frequently, certainly with previous global auroral imagers. As mentioned previously, the occurrence of CAAs is under-studied and a statistical survey is required, especially as this will provide new insights into the occurrence of DLR.

As an aside, we note that the magnitude of the B_X component of the IMF was significant at times, e.g. ≈ 10 nT during the first period of CAAs in Figure 3, and was near-zero at others, e.g. the last period of CAAs in Figure 4. This suggests that B_X does not

play a role in modulating the occurrence of (dual-) lobe reconnection and hence the occurrence of CAAs. This tallies with a lack of B_X control of the occurrence of HCAs reported by Bower, Milan, Paxton, and Anderson (2022).

Once DLR ceases the magnetosphere loses the trapped plasma and the polar cap reforms promptly, indicating the rapid opening of magnetic flux by magnetopause reconnection. This opening will occur most rapidly if the IMF is directed southwards and subsolar reconnection occurs, which will be accompanied by twin-cell convection in the polar ionosphere. However, as noted by Milan et al. (2022), it will also occur if the IMF is directed northwards with $|\theta| > 45°$ as single lobe reconnection will open a closed magnetosphere. Hence, CAAs are only seen for $|\theta| < 45°$.

Empirical magnetic field models, such as T96, do not reproduce a closed magnetosphere well, though closed NBZ magnetospheres are readily formed in simulations (e.g., Song et al., 1999; Siscoe et al., 2011; Wang et al., 2023). The magnetic field measurements made by C4/FGM and Geotail/MGF indicated that the B_X component was reduced when CAAs were present, with respect to when open lobe was observed. This indicates that the tail is somewhat deflated when it is closed (though it could also be in part because plasma pressure contributes to stress balance in the closed tail, rather than just magnetic pressure in the lobes). However, otherwise the field did not deviate markedly from the T96 predictions, indicating that if the magnetosphere is indeed closed, the magnetic structure near-Earth is not significantly modified, suggesting that the closed field lines stretch considerably further down-tail than the locations of C4 and Geotail. This is in contradiction to simulations which suggest that a closed magnetotail might be less than 20 R_E in length (Wang et al., 2023). Indeed, Milan, Carter, and Hubert (2020) estimated that closed field lines associated with transpolar arcs could extend as far as $X < -100\ R_E$. More work needs to be conducted in the distant magnetotail and with magnetospheric simulations to understand the magnetic topology of the closed magnetosphere.

4 Conclusions

We have investigated a fifteen-day period during which Cluster and Geotail sampled the magnetotail. Observations of the auroras by DMSP/SSUSI indicates that cusp-aligned arcs were present in the high latitude polar regions whenever the IMF clock angle was small, $|\theta| < 45°$, which during the study interval amounted to approximately 30% of the time. Simultaneous observations of ions and electrons by Cluster and Geotail show significant plasma densities ($n_i \approx n_e \approx 1\ \mathrm{cm}^{-3}$) in the tail during these intervals, even as far from the equatorial plane as $|Z| \approx 13\ R_E$. This region of the magnetotail would normally be devoid of plasma, being occupied by the open flux of the magnetotail lobe. The presence of counter-streaming ions and double loss-cone electrons suggest, instead, that the plasma was trapped, i.e., that the magnetic field was closed. This trapped plasma will provide a source for the CAA auroral emission, and as the auroral emission covered the polar regions, we further suggest that the magnetosphere was almost entirely closed. Coxon et al. (2021) recently showed that hot plasma consistent with trapping on closed field lines is frequently seen at $|Z| > 5\ R_E$ during northward IMF; here we have shown that CAAs are the auroral signature of this closed flux, and that at such times the magnetosphere is likely (almost) entirely closed. We believe that this closure is achieved by dual-lobe reconnection, as proposed by Milan, Carter, Bower, et al. (2020) and Milan et al. (2022). Our observations indicate that closure of the magnetosphere is a common occurrence.

5 Open Research

Data from the Cluster Ion Spectrometry (CIS) instrument, the Plasma Electron And Current Experiment (PEACE), and the Fluxgate Magnetometer (FGM) were accessed through the Cluster Science Archive (CSA, formerly Cluster Active Archive (Laakso

et al., 2010)) at `https://www.cosmos.esa.int/web/csa`, maintained by ESA/ESTEC. Geotail Magnetic Field Experiment (MGF) and Low Energy Particle (LEP) data were accessed through the DARTS Solar-Terrestrial Physics data portal (`https://www.darts .isas.jaxa.jp/stp/geotail/data.html`) maintained by ISAS/JAXA. The Defense Meteorological Satellite Program (DMSP) Special Sensor Ultraviolet Spectrographic Instrument (SSUSI) file type EDR-AUR data were obtained from JHU/APL (`http://ssusi .jhuapl.edu`, data version 0106, software version 7.0.0, calibration period version E0018). Advanced Magnetosphere and Planetary Electrodynamics Response Experiment (AMPERE) data were obtained from JHU/APL (`http://ampere.jhuapl.edu/dataget/index .html`) and processed using software provided (`http://ampere.jhuapl.edu/`). The high resolution (1-min) OMNI data used in this study were obtained from the NASA Goddard Space Flight Center Space Physics Data Facility OMNIWeb portal (`https://omniweb .gsfc.nasa.gov/form/om_filt_min.html`).

References

Anderson, B., Takahashi, K., & Toth, B. (2000). Sensing global Birkeland currents with Iridium® engineering magnetometer data. *Geophysical Research Letters*, *27*(24), 4045–4048. doi: https://doi.org/10.1029/2000GL000094

Balogh, A., Dunlop, M., Cowley, S., Southwood, D., Thomlinson, J., Glassmeier, K., ... others (1997). The Cluster magnetic field investigation. *Space Science Reviews*, *79*, 65–91. doi: https://doi.org/10.1023/A:1004970907748

Bower, G., Milan, S., Paxton, L., & Anderson, B. (2022). Occurrence statistics of horse collar aurora. *Journal of Geophysical Research: Space Physics*, e2022JA030385. doi: https://doi.org/10.1029/2022JA030385

Bower, G., Milan, S., Paxton, L., & Imber, S. (2022). Transpolar arcs: Seasonal dependence identified by an automated detection algorithm. *Journal of Geophysical Research: Space Physics*, *127*(1), e2021JA029743. doi: https://doi.org/10 .1029/2021JA029743

Carlson, H., & Cowley, S. (2005). Accelerated polar rain electrons as the source of sun-aligned arcs in the polar cap during northward interplanetary magnetic field conditions. *Journal of Geophysical Research: Space Physics*, *110*(A5).

Carter, J., Milan, S., Fogg, A., Paxton, L., & Anderson, B. (2018). The association of high-latitude dayside aurora with NBZ field-aligned currents. *Journal of Geophysical Research: Space Physics*, *123*(5), 3637–3645. doi: https://doi .org/10.1029/2017JA025082

Carter, J., Milan, S., Fogg, A., Sangha, H., Lester, M., Paxton, L., & Anderson, B. (2020). The evolution of long-duration cusp spot emission during lobe reconnection with respect to field-aligned currents. *Journal of Geophysical Research: Space Physics*, *125*, e2020JA027922. doi: https://doi.org/10.1029/ 2020JA027922

Chisham, G., Freeman, M., Abel, G., Lam, M., Pinnock, M., Coleman, I., ... Villain, J.-P. (2008). Remote sensing of the spatial and temporal structure of

magnetopause and magnetotail reconnection from the ionosphere. *Reviews of Geophysics*, *46*(1). doi: https://doi.org/10.1029/2007RG000223

Chisham, G., Freeman, M., Coleman, I., Pinnock, M., Hairston, M., Lester, M., & Sofko, G. (2004). Measuring the dayside reconnection rate during an interval of due northward interplanetary magnetic field. *Annales Geophysicae*, *22*(12), 4243–4258. doi: https://doi.org/10.5194/angeo-22-4243-2004

Chisham, G., Lester, M., Milan, S. E., Freeman, M., Bristow, W., Grocott, A., . . . others (2007). A decade of the Super Dual Auroral Radar Network (Super-DARN): Scientific achievements, new techniques and future directions. *Surveys in Geophysics*, *28*(1), 33–109. doi: https://doi.org/10.1007/s10712-007-9017-8

Cowley, S. (1981). Magnetospheric and ionospheric flow and the interplanetary magnetic field. *The Physical Basis of the Ionosphere in the Solar-Terrestrial System, AGARD-CP-295*, (4-1)–(4-14).

Cowley, S., & Lockwood, M. (1992). Excitation and decay of solar wind-driven flows in the magnetosphere-ionosphere system. *Annales Geophysicae*, *10*, 103–115.

Coxon, J., Fear, R., Reidy, J., Fryer, L., & Plank, J. (2021). Hot plasma in the magnetotail lobes shows characteristics consistent with closed field lines trapped in the lobes. *Journal of Geophysical Research: Space Physics*, *126*(9), e2021JA029516. doi: https://doi.org/10.1029/2021JA029516

Coxon, J., Milan, S., & Anderson, B. (2018). A review of Birkeland current research using AMPERE. *Electric Currents in Geospace and Beyond*, 257–278. doi: https://doi.org/10.1002/9781119324522.ch16

Cumnock, J., & Blomberg, L. (2004). Transpolar arc evolution and associated potential patterns. *Annales Geophysicae*, *22*(4), 1213–1231. doi: https://doi.org/10.5194/angeo-22-1213-2004

Cumnock, J., Sharber, J., Heelis, R., Blomberg, L. G., Germany, G., Spann, J., & Coley, W. (2002). Interplanetary magnetic field control of theta aurora development. *Journal of Geophysical Research: Space Physics*, *107*(A7), SIA–4. doi: https://doi.org/10.1029/2001JA009126

Dungey, J. (1961). Interplanetary magnetic field and the auroral zones. *Physical Review Letters*, *6*(2), 47.

Dungey, J. (1963). The structure of the exosphere, or adventures in velocity space. *Geophysics, The Earth's Environment*.

Escoubet, C., Fehringer, M., & Goldstein, M. (2001). Introduction the cluster mission. In *Annales geophysicae* (Vol. 19, pp. 1197–1200). doi: https://doi.org/10.5194/angeo-19-1197-2001

Fear, R. (2021). The northward IMF magnetosphere. *Magnetospheres in the Solar System*, 293–309. doi: https://doi.org/10.1002/9781119815624.ch19

Fear, R., & Milan, S. (2012a). The IMF dependence of the local time of transpolar arcs: Implications for formation mechanism. *Journal of Geophysical Research: Space Physics*, *117*(A3).

Fear, R., & Milan, S. (2012b). Ionospheric flows relating to transpolar arc formation. *Journal of Geophysical Research: Space Physics*, *117*(A9).

Fear, R., Milan, S., Maggiolo, R., Fazakerley, A., Dandouras, I., & Mende, S. (2014). Direct observation of closed magnetic flux trapped in the high-latitude magnetosphere. *Science*, *346*(6216), 1506–1510. doi: https://doi.org/10.1126/science.1257377

Frank, L., Craven, J., Burch, J., & Winningham, J. (1982). Polar views of the Earth's aurora with Dynamics Explorer. *Geophysical Research Letters*, *9*(9), 1001–1004. doi: https://doi.org/10.1029/GL009i009p01001

Frey, H. (2007). Localized aurora beyond the auroral oval. *Reviews of Geophysics*, *45*(1). doi: https://doi.org/10.1029/2005RG000174

Frey, H., Mende, S., Immel, T., Fuselier, S., Claflin, E., Gérard, J.-C., & Hubert, B. (2002). Proton aurora in the cusp. *Journal of Geophysical Research: Space Physics*, *107*(A7), SMP–2. doi: https://doi.org/10.1029/2001JA900161

Fryer, L., Fear, R., Coxon, J., & Gingell, I. (2021). Observations of closed magnetic flux embedded in the lobes during periods of northward imf. *Journal of Geophysical Research: Space Physics*, *126*(6), e2021JA029281. doi: https://doi.org/10.1029/2021JA029281

Fuselier, S., Trattner, K., Petrinec, S., & Lavraud, B. (2012). Dayside magnetic topology at the Earth's magnetopause for northward IMF. *Journal of Geophysical Research: Space Physics*, *117*(A8). doi: https://doi.org/10.1029/2012JA017852

Hones Jr, E., Craven, J., Frank, L., Evans, D., & Newell, P. (1989). The horse-collar aurora: A frequent pattern of the aurora in quiet times. *Geophysical Research Letters*, *16*(1), 37–40. doi: https://doi.org/10.1029/GL016i001p00037

Hosokawa, K., Kullen, A., Milan, S., Reidy, J., Zou, Y., Frey, H. U., ... Fear, R. (2020). Aurora in the polar cap: A review. *Space Science Reviews*, *216*(1), 15. doi: https://doi.org/10.1007/s11214-020-0637-3

Hosokawa, K., Moen, J., Shiokawa, K., & Otsuka, Y. (2011). Motion of polar cap arcs. *Journal of Geophysical Research: Space Physics*, *116*(A1). doi: https://doi.org/10.1029/2010JA015906

Huang, C.-S., Sofko, G., Koustov, A., Andre, D., Ruohoniemi, J., Greenwald, R., & Hairston, M. (2000). Evolution of ionospheric multicell convection during northward interplanetary magnetic field with $|B_z/B_y| > 1$. *Journal of Geophysical Research: Space Physics*, *105*(A12), 27095–27107. doi: https://doi.org/10.1029/2000JA000163

Iijima, T., & Potemra, T. (1976). The amplitude distribution of field-aligned currents at northern high latitudes observed by Triad. *Journal of Geophysical Research*, *81*(13), 2165–2174. doi: https://doi.org/10.1029/JA081i013p02165

Iijima, T., Potemra, T., Zanetti, L., & Bythrow, P. (1984). Large-scale Birkeland currents in the dayside polar region during strongly northward IMF: A new Birkeland current system. *Journal of Geophysical Research: Space Physics*, *89*(A9), 7441–7452. doi: https://doi.org/10.1029/JA089iA09p07441

Imber, S., Milan, S., & Hubert, B. (2006). The auroral and ionospheric flow signatures of dual lobe reconnection. *Annales Geophyiscae*, *24*(11), 3115–3129. doi: https://doi.org/10.5194/angeo-24-3115-2006

Ismail, S., Wallis, D., & Cogger, L. (1977). Characteristics of polar cap Sun-aligned arcs. *Journal of Geophysical Research*, *82*(29), 4741–4749. doi: https://doi.org/10.1029/JA082i029p04741

Johnstone, A., Alsop, C., Burge, S., Carter, P., Coates, A., Coker, A., ... others (1997). Peace: A plasma electron and current experiment. *Space Science Reviews*, 351–398. doi: https://doi.org/10.1023/A:1004938001388

King, J., & Papitashvili, N. (2005). Solar wind spatial scales in and comparisons of hourly Wind and ACE plasma and magnetic field data. *Journal of Geophysical Research: Space Physics*, *110*(A2). doi: https://doi.org/10.1029/2004JA010649

Kokubun, S., Yamamoto, T., Acuña, M., Hayashi, K., Shiokawa, K., & Kawano, H. (1994). The GEOTAIL magnetic field experiment. *Journal of geomagnetism and geoelectricity*, *46*(1), 7–21. doi: https://doi.org/10.5636/jgg.46.7

Kullen, A., Brittnacher, M., Cumnock, J., & Blomberg, L. (2002). Solar wind dependence of the occurrence and motion of polar auroral arcs: A statistical study. *Journal of Geophysical Research: Space Physics*, *107*(A11), 13–1. doi: https://doi.org/10.1029/2002JA009245

Laakso, H., Perry, C., McCaffrey, S., Herment, D., Allen, A., Harvey, C., ... Turner, R. (2010). *Cluster active archive: Overview*. Springer.

Lockwood, M., & Cowley, S. (1992). Ionospheric convection and the substorm cycle. *Proceedings of the International Conference on Substorms (ICS-1)*, 99–109.

Mailyan, B., Shi, Q., Kullen, A., Maggiolo, R., Zhang, Y., Fear, R., ... others (2015). Transpolar arc observation after solar wind entry into the high-latitude

magnetosphere. *Journal of Geophysical Research: Space Physics*, *120*(5), 3525–3534.

Milan, S., Bower, G., Carter, J., Paxton, L., Anderson, B., & Hairston, M. (2022). Lobe reconnection and cusp-aligned auroral arcs. *Journal of Geophysical Research: Space Physics*, *127*(6), e2021JA030089. doi: https://doi.org/10.1029/2021JA030089

Milan, S., Carter, J., Bower, G., Imber, S., Paxton, L., Anderson, B., . . . Hubert, B. (2020). Dual-lobe reconnection and horse-collar auroras. *Journal of Geophysical Research: Space Physics*, *125*(10), e2020JA028567. doi: https://doi.org/10.1029/2020JA028567

Milan, S., Carter, J., & Hubert, B. (2020). Probing the magnetic structure of a pair of transpolar arcs with a solar wind pressure step. *Journal of Geophysical Research: Space Physics*, *125*(2), e2019JA027196.

Milan, S., Carter, J., Sangha, H., Bower, G., & Anderson, B. (2021). Magnetospheric flux throughput in the dungey cycle: Identification of convection state during 2010. *Journal of Geophysical Research: Space Physics*, *126*(2), e2020JA028437. doi: https://doi.org/10.1029/2020JA028437

Milan, S., Cowley, S., Lester, M., Wright, D., Slavin, J., Fillingim, M., . . . Singer, H. (2004). Response of the magnetotail to changes in the open flux content of the magnetosphere. *Journal of Geophysical Research: Space Physics*, *109*(A4). doi: https://doi.org/10.1029/2003JA010350

Milan, S., Hubert, B., & Grocott, A. (2005). Formation and motion of a transpolar arc in response to dayside and nightside reconnection. *Journal of Geophysical Research: Space Physics*, *110*(A1). doi: https://doi.org/10.1029/2004JA010835

Milan, S., Lester, M., Cowley, S., & Brittnacher, M. (2000). Dayside convection and auroral morphology during an interval of northward interplanetary magnetic field. *Annales Geophysicae*, *18*(4), 436–444. doi: https://doi.org/10.1007/s00585-000-0436-9

Milan, S., Lester, M., Cowley, S., Oksavik, K., Brittnacher, M., Greenwald, R., . . . Villain, J.-P. (2003). Variations in the polar cap area during two substorm cycles. *Annales Geophysicae*, *21*(5), 1121–1140.

Milan, S., Provan, G., & Hubert, B. (2007). Magnetic flux transport in the Dungey cycle: A survey of dayside and nightside reconnection rates. *Journal of Geophysical Research: Space Physics*, *112*(A1). doi: https://doi.org/10.1029/2006JA011642

Mukai, T., Machida, S., Saito, Y., Hirahara, M., Terasawa, T., Kaya, N., . . . Nishida, A. (1994). The low energy particle (LEP) experiment onboard the Geotail satellite. *Journal of geomagnetism and geoelectricity*, *46*(8), 669–692. doi: https://doi.org/10.5636/jgg.46.669

Nishida, A. (1994). *The geotail mission* (Vol. 21) (No. 25). Wiley Online Library.

Øieroset, M., Raeder, J., Phan, T., Wing, S., McFadden, J., Li, W., . . . Balogh, A. (2005). Global cooling and densification of the plasma sheet during an extended period of purely northward IMF on October 22–24, 2003. *Geophysical Research Letters*, *32*(12).

Paxton, L., Meng, C.-I., Fountain, G., Ogorzalek, B., Darlington, E., Gary, S., . . . others (1992). Special sensor ultraviolet spectrographic imager: An instrument description. In *Instrumentation for planetary and terrestrial atmospheric remote sensing* (Vol. 1745, pp. 2–15). doi: https://doi.org/10.1117/12.60595

Paxton, L., Schaefer, R., Zhang, Y., & Kil, H. (2017). Far ultraviolet instrument technology. *Journal of Geophysical Research: Space Physics*, *122*(2), 2706–2733. doi: https://doi.org/10.1002/2016JA023578

Paxton, L., & Zhang, Y. (2016). Far ultraviolet imaging of the aurora. In *Space weather fundamentals* (pp. 213–244). CRC Press.

Paxton, L., Zhang, Y., Kil, H., & Schaefer, R. (2021). Exploring the upper atmo-

sphere: Using optical remote sensing. *Upper Atmosphere Dynamics and Energetics*, 487–522. doi: https://doi.org/10.1002/9781119815631.ch23

Reidy, J., Fear, R., Whiter, D., Lanchester, B., Kavanagh, A., Price, D. J., . . . Paxton, L. (2020). Multiscale observation of two polar cap arcs occurring on different magnetic field topologies. *Journal of Geophysical Research: Space Physics*, *125*(8), e2019JA027611.

Rème, H., Bosqued, J., Sauvaud, J., Cros, A., Dandouras, J., Aoustin, C., . . . others (1997). The cluster ion spectrometry (cis) experiment. *The cluster and phoenix missions*, 303–350. doi: https://doi.org/10.1007/978-94-011-5666-0_12

Rich, F., & Hairston, M. (1994). Large-scale convection patterns observed by DMSP. *Journal of Geophysical Research: Space Physics*, *99*(A3), 3827–3844. doi: https://doi.org/10.1029/93JA03296

Shi, Q., Zong, Q.-G., Fu, S., Dunlop, M., Pu, Z., Parks, G., . . . others (2013). Solar wind entry into the high-latitude terrestrial magnetosphere during geomagnetically quiet times. *Nature communications*, *4*, 1466.

Siscoe, G., Farrugia, C., & Sandholt, P. (2011). Comparison between the two basic modes of magnetospheric convection. *Journal of Geophysical Research: Space Physics*, *116*(A5). doi: https://doi.org/10.1029/2010JA015842

Siscoe, G., & Huang, T. (1985). Polar cap inflation and deflation. *Journal of Geophysical Research: Space Physics*, *90*(A1), 543–547.

Song, P., DeZeeuw, D., Gombosi, T., Groth, C., & Powell, K. (1999). A numerical study of solar wind-magnetosphere interaction for northward interplanetary magnetic field. *Journal of Geophysical Research: Space Physics*, *104*(A12), 28361–28378. doi: https://doi.org/10.1029/1999JA900378

Taylor, M., Lavraud, B., Escoubet, C., Milan, S., Nykyri, K., Dunlop, M., . . . others (2008). The plasma sheet and boundary layers under northward IMF: A multi-point and multi-instrument perspective. *Advances in Space Research*, *41*(10), 1619–1629.

Tsyganenko, N. (1995). Modeling the earth's magnetospheric magnetic field confined within a realistic magnetopause. *Journal of Geophysical Research: Space Physics*, *100*(A4), 5599–5612. doi: https://doi.org/10.1029/94JA03193

Wang, X.-Y., Zhang, Q.-H., Wang, C., Zhang, Y.-L., Tang, B.-B., Xing, Z.-Y., . . . others (2023). Unusual shrinkage and reshaping of earth's magnetosphere under a strong northward interplanetary magnetic field. *Communications Earth & Environment*, *4*(1), 31. doi: https://doi.org/10.1038/s43247-023-00700-0

Waters, C., Anderson, B., & Liou, K. (2001). Estimation of global field aligned currents using the Iridium® system magnetometer data. *Geophysical Research Letters*, *28*(11), 2165–2168. doi: https://doi.org/10.1029/2000GL012725

Zhang, Q.-H., Zhang, Y.-L., Wang, C., Lockwood, M., Yang, H.-G., Tang, B.-B., . . . others (2020). Multiple transpolar auroral arcs reveal insight about coupling processes in the Earth's magnetotail. *Proceedings of the National Academy of Sciences*, *117*(28), 16193–16198. doi: https://doi.org/10.1073/pnas.2000614117

Zhang, Y., Paxton, L., Zhang, Q.-H., & Xing, Z. (2016). Polar cap arcs: Sun-aligned or cusp-aligned? *Journal of Atmospheric and Solar-Terrestrial Physics*, *146*, 123–128. doi: https://doi.org/10.1016/j.jastp.2016.06.001